Pergamon

Int. J. Heat Mass Transfer. Vol. 41, No. 3, pp. 613–623, 1998

Printed in Great Britain
0017-9310/98 $19.00+0.00

PII: S0017-9310(97)00105-1

Heat transfer and life of metal cutting tools in turning

HERCHANG AY
Department of Mechanical Engineering, Nan-Tai Institute of Technology, Tainan, Taiwan, Republic of China

and

WEN-JEI YANG†
Department of Mechanical Engineering and Applied Mechanics, University of Michigan, Ann Arbor, MI 48109, U.S.A.

(*Received* 15 *February* 1997 *and in final form* 7 *April* 1997)

Abstract—An experimental study is performed using both thermocouples and infrared thermovision to monitor timewise temperature variations of the tool and workpiece in orthogonal cutting. A semi-empirical formula is derived to express the temperature–time history of the tool surface, using a local element lumped conduction equation with experimental data-fitting. Infrared thermovision identifies the location of the maximum tool temperature slightly inward from the cutting edge. An optical and electronic microscope reveals the formation of micropits, the origin of flank and rake wear that originates in the region of surrounding the maximum tool temperature. It is disclosed that the progression of wears is accompanied by a consistent increase in the tool temperature which in turn accelerates the wearing process. Chip geometry is found to affect local steady-state temperatures in the cutting tool. For cast iron and copper, chip geometry may causes a zig-zag variation in the steady-state temperature with respect to the rate of material removal for a change in the feed. The study sheds light on the causes of roughness of surfaces cut with a hard tool and may thus serve as the first step in the investigation of surface machining. © 1997 Elsevier Science Ltd.

INTRODUCTION

With increasing cutting speeds used in modern machining operations, the thermal aspects of cutting become more and more important. It not only directly influences the rate of tool wear, but also will affect machining precision recognized as thermal expansion [1–5] and the roughness of the surface finish. Hence, one needs to accurately evaluate the rate of cutting heat generation and temperature distributions on the machining surface. The major methods of measuring cutting temperatures were reviewed in Ay [6] and classified as:

(1) Tool–workpiece thermocouple techniques. This method is based on the fact that the tool and workpiece are different materials, and the interface between the tool and the chip is at an elevated temperature [7, 8]. Braiden [9] stated a concern with the measurement of tool–chip interface temperature during intermittent cutting, using tungsten carbide tools.
(2) Thermocouple-insert techniques. Küster [10] inserted thermocouple wires into carbide tips for mapping the temperature field using an extremely tedious procedure involving many tools with thermocouples mounted at different points. Usui *et al.* [11] inserted 0.01 mm diameter platinum wire into a quartz tube embedded in a divided carbide tool-tip for measuring the temperature on the tool face.
(3) Thermovision techniques. Schwerd [12] measured infrared radiation from tool, work and chip during orthogonal cutting to determine the temperature field on the outside surfaces of these regions. Hollander [13] and Chao *et al.* [14] utilized infrared pyrometers, Trigger [15] employed a lead sulfide radiation sensor, Boothroyd [16] used a microdensitometer for measuring the point-to-point intensity of radiation with the aid of a suitable negative calibration, and Bicket and Widmer [17] and Lenz [18] measured radiant heat from holes made on the workpiece and tool.
(4) Metallographic techniques. Of course, a family of curves need to be obtained by calibrating the hardness against the temperature and its time of heating for any tool material first. The temperature of the heat-affected region in the tool can be defined by measuring the hardness and time of heating [19, 20].

† Author to whom correspondence should be addressed.

NOMENCLATURE

A	surface area [m^2]
a	half chip-tool contact width [mm]
C	empirical parameter [°C]
C_P	specific heat [kJ kg^{-1} $°C^{-1}$]
f	feed (rate) [mm rev^{-1}]
h	heat transfer coefficient [W m^{-2} $°C^{-1}$]
k	thermal conductivity [W m^{-1} $°C^{-1}$]
q	frictional heat per length [W]
T	temperature [°C]
t	time [s]
V	cutting speed [m s^{-1}]
w	depth of cut [mm]

Greek symbols

ρ	density [kg m^{-3}]
Γ	tool life
τ	time constant [s]
υ	volume [m^3]

Subscripts

1	insert (tool)
2	workpiece
∞	ambient.

(5) Thermosensitive paints or liquid crystals were used by Schallbrock and Lang [21], Pahlitzsch and Helmerdig [22], Bickel and Widmer [17], and others in temperature measurements during cutting processes. This technique is limited to accessible surfaces under steady-state conditions and is incapable of giving accurate temperatures at actual wear surfaces.

Most of the efforts in studying heat transfer in cutting tools have been directed toward determining temperature distributions in the chip and workpiece, through which heat transfer in the cutting tool may be indirectly evaluated. Nevertheless, many assumptions imposed, in order to simplify theoretical models, have jeopardized their validates. In contrast, little attention was focused on the direct evaluation of the heat transfer process in the cutting tool, either experimentally or theoretically. The main obstacle involved difficulties in temperature measurements and uncertainties in theoretical modeling. Ay *et al.* [23] developed a modified thermocouple-insert method to monitor the time history of tool temperature in a cutting process. Extra-fine thermocouples were inserted into the tool tip and connected to a data acquisition system for recording the real-time temperature variation at strategic locations on the tool surface.

In this study, an infrared thermographic system was developed for simultaneous and synchronized measurements of the temperature distribution by calibrating against thermocouples. Four different workpieces were machined by using two kinds of tool inserts, under various operating conditions to investigate the temperature distribution of the carbide inserts and how heat transfer may affect tool wears. In addition, an optical and electronic microscope was employed for microscopic investigation of tool surfaces in the post-cutting stage.

EXPERIMENTAL APPARATUS

The test setup used in the modified thermocouple-insert method [23] consisted of a lathe for machining a workpiece and a thermocouple data acquisition system for gathering, monitoring, displaying and ana-

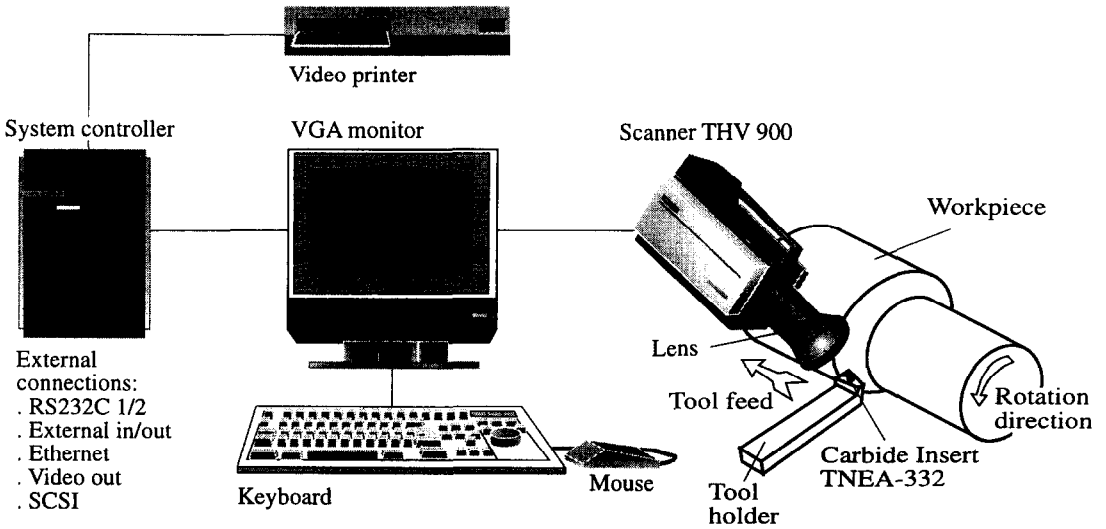

Fig. 1. Infrared system thermovision.

lyzing temperature data. The thermocouple data acquisition system included two white box plug-in interfaces with 12-bit A/D resolution and 16 digital I/O lines for a Macintosh II computer, and was used for digital recordings of the tool temperatures monitored by the thermocouples inserted into the cutting tool. The accuracy of temperature measurements using the thermocouple data acquisition system for the study was ± 1.4°C.

The experimental apparatus for infrared temperature measurements used in AGEMA infrared system (thermovision model 900). A complete, standalone temperature measurement workstation, the Thermovision 900 shown in Fig. 1, is comprised of a precision optical scanner, a dedicated system controller, lens, a keyboard, a mouse, and a VGA monitor. Note that the optical scanner was placed directly over the tool–chip contact zone during cutting. Temperature measurements by means of the scanner had an accuracy of ± 1°C.

With the instalment of both the thermocouple- and infrared-data acquisition systems, a simultaneous measurement of both local (at the locations of the thermocouples tips) and global (under the scanner lens) temperatures can be accomplished. An optical image-processing system provided a high resolution and sharp image for visualizing micro phenomena on the tool surface after the cutting operation. It included an optical and electronic microscope, CCTV camera/camera kit, high resolution color display, Macintosh Quadra 950, and software of Video Image Capture, as schematically shown in Fig. 2. The optical fiberscope with a light source might be used for a close observation of specimens with flexible movement and adjustment in any direction and at any location.

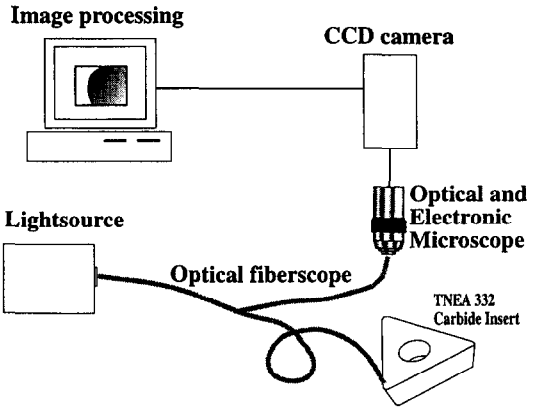

Fig. 2. Experimental set-up for micrograph of tool surface.

MATERIALS AND EXPERIMENTAL DESIGNS

The work materials cut were 6061 aluminum, copper, case iron, and AISI 1045 steel, all in the form of a cylindrical rod. Some properties of these materials are presented in Table 1 [24]. Grades VC2 and VC7 of TNEA 332 uncoated carbide inserts, composed of tungsten carbide cemented with a cobalt binder, were employed in cutting the work materials. Some properties of the inserts are listed in Table 2.

Nine type-K fine thermocouples with calibration were positioned while the thermocouple measurement was imposed, three each at the edge of three surfaces of a tool-insert [23]. Before the experimental tests of the infrared temperature measurement, it is necessary to provide the object parameters, including the emissivity, object distance, relative humidity, atmospheric temperature, and reflected ambient temperature, for the system performance. It maybe noted that a laboratory calibration is needed to determine the emissivity of tested materials. In this study, a portion of the workpiece and all tool inserts were painted with a black paint of known emissivity of 0.96.

The test conditions are summarized in Table 3. Fractional factorial designs are used to vary the cutting speed (V), feed rate (f), and depth of cut (w)

Table 1. Some physical properties of workpieces

	6061 aluminum	Copper	Cast iron	1045 steel
Specific gravity	2.7	8.96	7.2–7.4	7.86
Density (kg m^{-3})	2700	8960	7200–7400	7860
Solidus/liquidus (°C)	552–652	1083	1150–1450	1470–1500
Thermal conductivity	190–210(†)	385	46–63	41.9
(W m^{-1} °C^{-1})	170–200(‡)			
Young's modulus of elasticity (N m^{-2})	$65.5–68.9 \times 10^9$	110×10^9	$138–152 \times 10^9$	—

† annealed.
‡ solution treated and aged.

Table 2. Normal physical properties of insert

Valenite grade	Hardness [Ra]	Density [g cc^{-1}]	Thermal conductivity [W m^{-1} K^{-1}]	Specific heat [J kg^{-1} K^{-1}]
VC2	92.0	14.85	112.5	208
VC7	92.1	12.30	52.1	118

Table 3. Summary of the cutting conditions

Grade—type inserts	VC2, VC7
Flat insert	TNEA 332
Rake angle	$-7°$
Clearance angle	$7°$
Cutting speed	0.89, 1.93, 3.00, 3.81 m s^{-1}
Feed rate	0.05, 0.08, 0.11, 0.17 mm rev^{-1}
Depth of cut	0.25, 0.51, 0.76 mm
Cutting edge nose radius	0.80 mm
Workpiece	6061 aluminum, copper, cast iron, AISI 1045 steel
Lubrication	none

over a broad range, when cutting cast iron, 1045 steel, copper and 6061 aluminum. Four levels of cutting speed (0.89, 1.93, 3.00 and 3.81 m s^{-1}) combined with three feed rates (0.05, 0.08 and 0.11 mm rev^{-1}) at a cutting depth of 0.25 mm, fixed rake angle of $-7°$, and a leading angle of $0°$ were tested.

RESULTS AND DISCUSSION

During a cutting process, the force exerted by a motor is converted into heat at a contact area between the tool edge and the chip which diffuses throughout the cutting tool. The local heat process can be classified into three stages: early, transition, and late stages. In the early stage, only the energy transferred is absorbed, resulting in a rapid and temporal increase in the local temperature. In the transition stage, however, the energy transferred is partially absorbed to raise its enthalpy and is then partially diffused into the neighboring domain. This results in a temporarily exponential increase in the local temperature which then asymptotically approaches its final steady value, i.e. late stage.

The temporal variations of tool temperatures at the nine locations, indicated from TC1 through TC9, were measured in real-time and plotted by the thermocouple data acquisition system [23]. Typical results are also presented in Fig. 3 for the tool with VC7 insert in cutting cast iron, AISI 1045 steel, 6061 aluminum, and copper, respectively, under the identical operating conditions of $V = 1.93$ m s^{-1}, $f = 0.05$ mm rev^{-1} and $w = 0.25$ mm by using thermocouple measurements. Parts (b), (c) and (d) of the figures present the temperature response curves of (TC1 to TC3), (TC4 to TC6) and (TC7 to TC9), respectively. Other plots for cutting AISI 1045 steel, 6061 aluminum and copper [6, 23] are compared with Fig. 3. It is disclosed that the temperature response is temporally exponential with fluctuations. Comparison with the temperature response curves at relative locations on the cutting tool, the amplitude of the fluctuations diminishes with increasing distance from the heat source (the contact zone between the cutting tool and the workpiece).

An examination of the test results reveals an exponential form of each temperature response curve. The surface temperature in dimensionless form is obtained as timewisely exponential and can be approximated in the following form:

$$\frac{T-T_\infty}{C} = 1-\exp\left(-\frac{t}{\tau}\right). \tag{1}$$

Here, τ is the time constant defined as $\tau \equiv \rho_1 v_1 C_{P_1}/hA_1$ and the parameter C takes the form of

$$C = \frac{q}{k_1 2a} \tag{2}$$

assuming that it is dominated by the frictional heat q. Here, k_1 denotes the thermal conductivity of the insert and 2a is the chip-tool contact width. The values of C and τ are determined by curve fitting the experimental data for individual cutting conditions and the different workpieces, as shown in part (a) of Fig. 3.

The extent of temperature oscillations varies with the work materials and is most severe in cutting copper, followed by 6061 aluminum, AISI 1045 steel, and then cast iron. These temperature fluctuations are caused by chip formation, which raises the local temperature upon contact with the work material. The difference in the extent of temperature oscillations can be attributed to differences in chip shape and size during machining operations, and the metal properties of the work materials. The chip formation involves a shearing of the work material in the region of a plane extending from the tool edge to the position where the upper surface of the chip leaves the work surface, known as shear region or the primary deformation region [25]. A very large amount of strain occurs in this region in a very short span of time, and not all metals or alloys can withstand this strain without fracturing.

Figure 4 depicts the effects of operating conditions (for a depth of cut fixed at 0.25 mm) of steady-state temperatures in the four work materials on (a) the cutting speed, and (b) the feed. It is essentially a plot of equation (1). Thus, Fig. 4(a) is similar to that of parameter C in equation (1). One observes, in Fig. 4(a), that the steady-state temperature in the work materials producing continuous chips, such as copper and aluminum, increases with the cutting speed, and eventually levels off at high cutting speeds. In contrast, the steady-state temperature in the work materials producing discontinuous chips, cast iron and steel continues to increase proportionally to the cutting speed. The same tendency appears in Fig. 4(b) for the effects of feed on steady-state temperatures.

Figure 5 shows the effects of the rate of metal removal on steady-state temperature in the work materials. The product of the cutting speed (V), feed (f) and depth of cut (w) determines the rate of metal removal, a parameter often used in measuring the efficiency of a cutting operation. The cutting speed and feed are the two most important parameters which can be adjusted by the operator to achieve optimum cutting conditions. The depth of cut is often fixed by

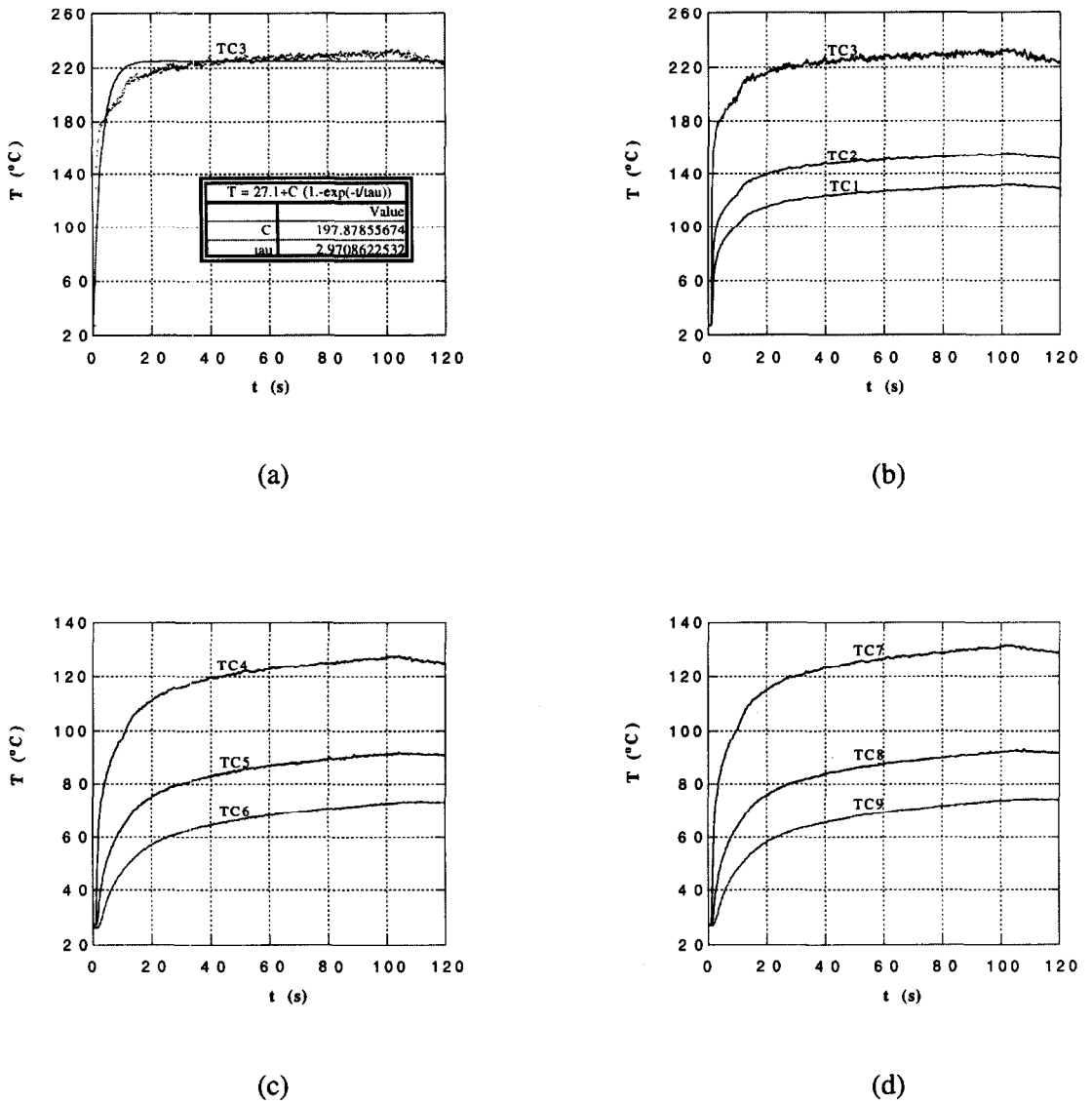

Fig. 3. (a) Comparison of semi-empirical model (solid line) with temperature measured at TC3 and temperature–time history in early and late stages; (b) at TC1, TC2, TC3; (c) at TC4, TC5, TC6; (d) at TC7, TC8, TC9 and for $V = 1.93$ m s^{-1}, $f = 0.11$ mm rev^{-1}, $w = 0.25$ mm, and cast iron.

the required size of the product. The results of Fig. 5 show that a high efficiency of cutting operation will increase the temperature of the tool and decrease the life of the tool (shown in Fig. 6) for most work materials over a wide range of cutting conditions. It is seen in Fig. 5 that the steady-state temperature T for cast iron increases with the rate of metal removal Vfw. Beyond point a, a sudden drop in the T-curve indicates a change (increase) in the feed f. The curve rises with Vfw at the new feed. Beyond point b, another step decrease in the T-curve, forms a zig-zag variation in the T vs Vfw characteristics. In the case of copper, a change in the feed also causes a zig-zag form of the T–Vfw relationship, a sudden increase in T at a f change (increase) followed by a gradual decrease, which is opposite to that for cast iron. This peculiar phenomenon is not observed in steel and aluminum.

The values of C obtained from correlating the temperature response curves are plotted in Fig. 6, as a function of the cutting speed V for cast iron, AISI 1045 steel, copper, and 6061 aluminum. All curves are nearly straight and can be grouped into two categories: cast iron and AISI 1045 steel are characterized by steeper slopes, practically parallel. On the other hand, copper and 6061 aluminum have flatter slopes at a higher cutting speed. The curve for copper is nearly horizontal due to its high thermal conductivity. Aluminum has a flatter C curve than steel and cast iron, whose thermal conductivities are close to each other, but less than copper. A working material with a high thermal conductivity can quickly dissipate

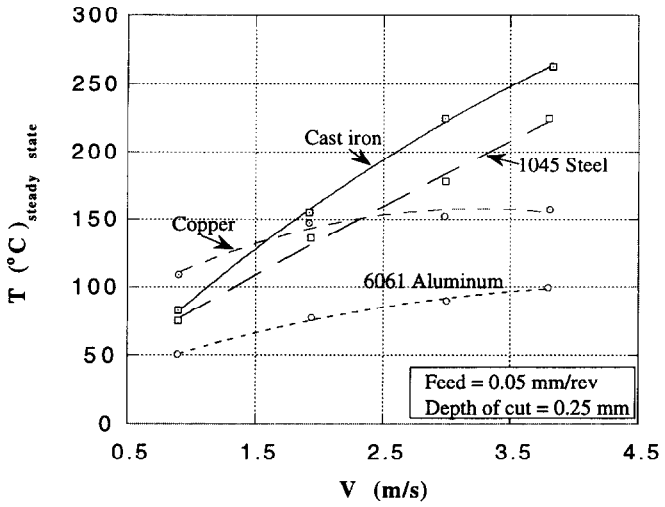

(a)

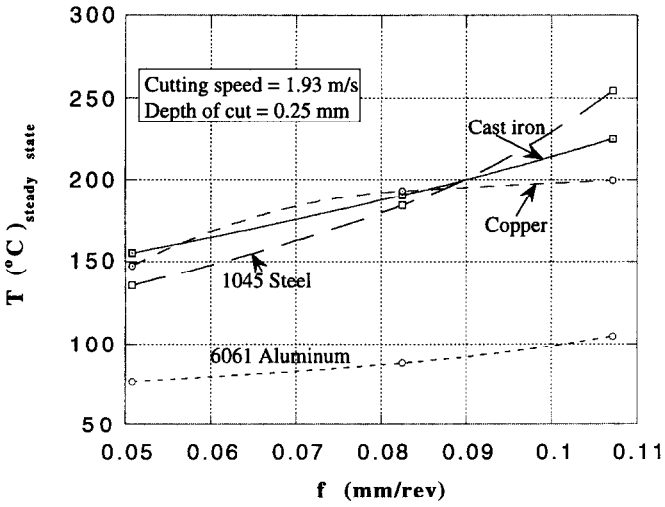

(b)

Fig. 4. Effects of operating condition on steady-state temperature in the work materials: (a) the cutting speed; and (b) the feed.

the heat generated by shear and friction away from the cutting area. The right ordinate of Fig. 6 gives the tool life Γ whose magnitude increases in an upward direction. Tool life is defined as the cutting time to produce an amount of flank wear (e.g. 0.75 mm) in conventional study. For all four materials, the Γ–V relationship confirms Taylor's equation for tool life, which is inversely proportional to the cutting speed. Note that we only determine (or sensor) the tool temperature around the cutting zone during machining, the tool life (cutting time) could be predicted after calibration with the curves of the Γ–V relationship.

The results of the infrared thermovision for steady-state temperature distribution on the surface of a tool are presented in Fig. 7 which include the thermograms in part (a) and associated line graphs, shown in part (b). A 16-step color palette (approximately 20°C per step) was used in the thermograms so that temperatures throughout the insert can easily be correlated. The line graphs are the temperature profiles along lines LI01 (blue), LI02 (orange) and LI03 (green) shown on the thermogram in Fig. 7. Note that the lines, LI01 and LI03, are located along the edges of the insert for comparison with the results obtained by thermocouples TC4–6 and TC7–9, respectively. The temperature gradient on the rake face has the same pattern as that obtained by the thermocouple measurements and is very steep near the cutting edge

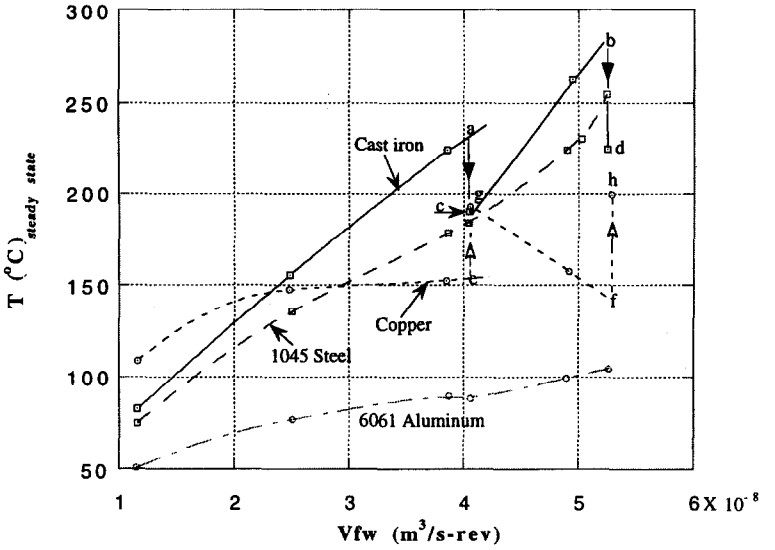

Fig. 5. Effects of the rate of metal removal on steady-state temperature in the work materials.

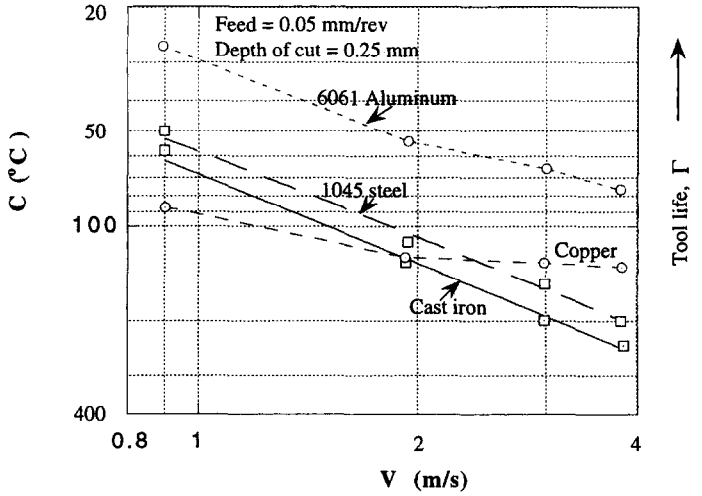

Fig. 6. C value and tool life vs cutting speed for cast iron, AISI 1045 steel, copper and 6061 aluminum.

of the tool due to a large amount of heat transferred into the insert through a very small contact area over short time intervals. The maximum temperature in each thermal image is also shown in the thermograms, noted below the image following the word 'ISO1' [for example, for INS 2.1 the hottest temperature is 410°C in Fig. 7(a)]. It is found from the thermograms that a significant change in the temperature distribution in the tool insert depends on the chip formation (not shown). For the same form of chip produced, the thermal patterns on surface of the tool insert are similar.

Figure 8 shows the steady temperature distribution in the VC7 insert obtained by combining the results from the infrared and thermocouple tests. It shows typical temperature contours on the rake and flank face of a TNEA 332 carbide insert for $V = 1.93\ \text{m s}^{-1}$, $f = 0.11\ \text{mm rev}^{-1}$, and $w = 0.25$ mm in AISI 1045 steel cutting. The highest temperature is observed to occur at some distance from the cutting edge of the rake face. One explanation of this behavior is that the tool–chip contact area combines the heat due to the frictional effect on the tool–chip contact interface and the heat from the primary deformation zone carried by the chip flow. Since the heat, due to plastic work generated in the primary deformation zone, is largely convected with material flow, only a small amount of heat is conducted into the workpiece. Therefore, the temperature distribution at some distance away from the primary deformation zone in the workpiece has no appreciable change (not shown). Note that the temperatures in the tool insert may be lower compared to existing numerical results, which always impose insulated boundary conditions on the flank face of the tool and parts of the rake face that do not contact the chip.

It is important to know that conditions exist at the interface between tool and workpiece during cutting.

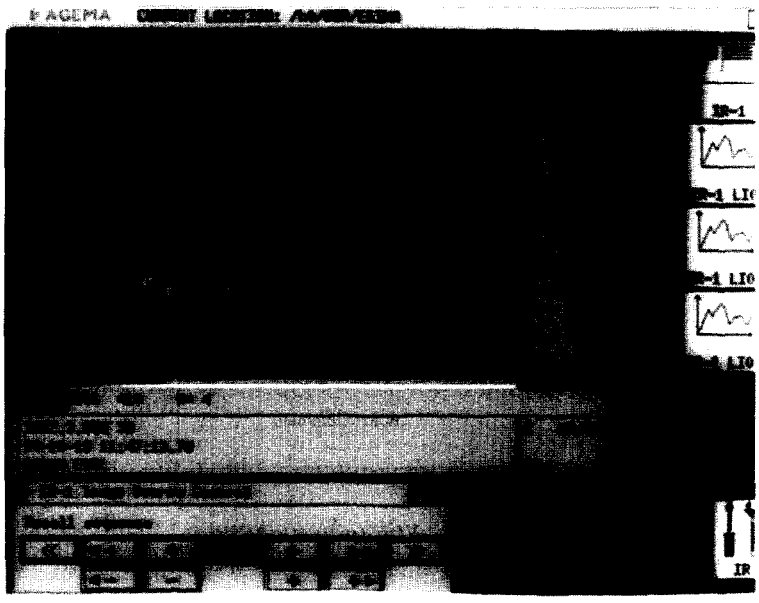

(a)

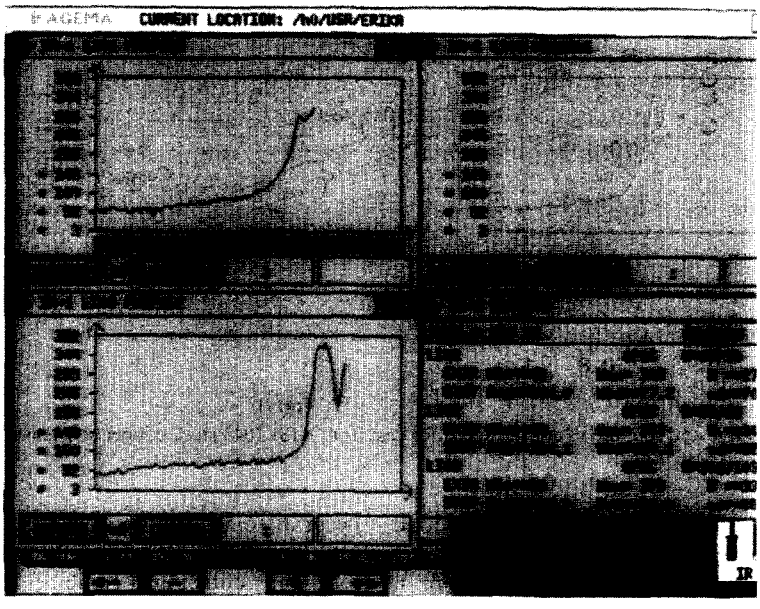

(b)

Fig. 7. Correlation of steady-state temperature profiles: (a) thermograms; (b) line graphs for $V = 1.93$ m s^{-1}, $f = 0.11$ mm rev^{-1}, $w = 0.25$ mm, and VC7 insert for cutting AISI 1045 steel.

Figure 9 is a photomicrograph (× 200) of a section on the rake face of a tungsten carbide tool used to cut copper. The white (light) area is the residual copper layer, which is attached to the tool rake face (horizontal surface of the insert), the cutting edge (not shown), and down the worn flank (not shown). It should be noted that the copper adhering to the tool had recrystallized and the contact between the two surfaces became continuous, in spite of the uneven surface of the tool, which could make sliding impossible.

Many investigations have shown the two surfaces to be interlocked, with the adhering metal penetrating both major and minor irregularities in the tool surface. When cutting gray cast iron, much less adhesion might be expected than when the work material is copper, because of the segmented chips and the presence of graphite in the gray cast iron. Also, the direction of

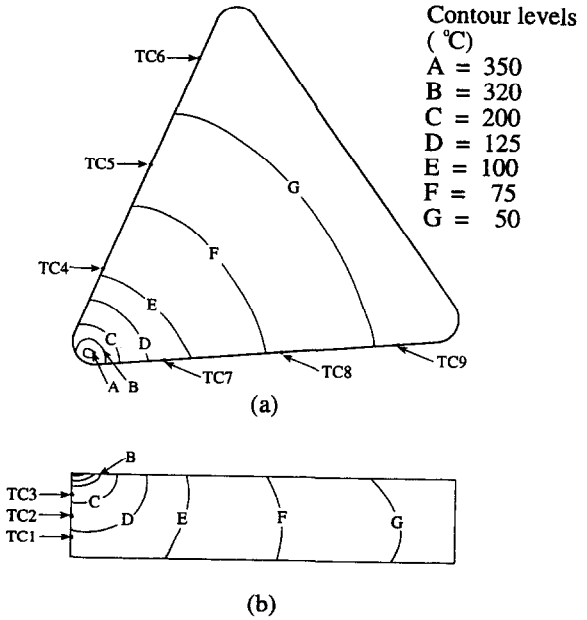

Fig. 8. Temperature distribution in grade VC7, TNEA 332 insert: (a) rake face; and (b) flank face for $V = 1.93$ m s^{-1}, $f = 0.11$ mm rev^{-1}, $w = 0.25$ mm, cutting AISI 1045 steel.

chip flow can obviously be obtained by means of observing the adhering metal flow on the rake face.

Another interesting disclosure is the formation of black cavities called micropits, two of which are found in the bottom rim of the rake face (Fig. 9). They are formed from whole grains or fragments of carbon grains being broken away. Both the number and size of micropits increase with cutting time, producing two kinds of wear. If they formed along the cutting edge, it results in groove wear. Whereas, if the micropits are produced on the crater face (not shown), eventually fragments of the tool material of microscopic size would be torn from the surface, resulting in crater wear.

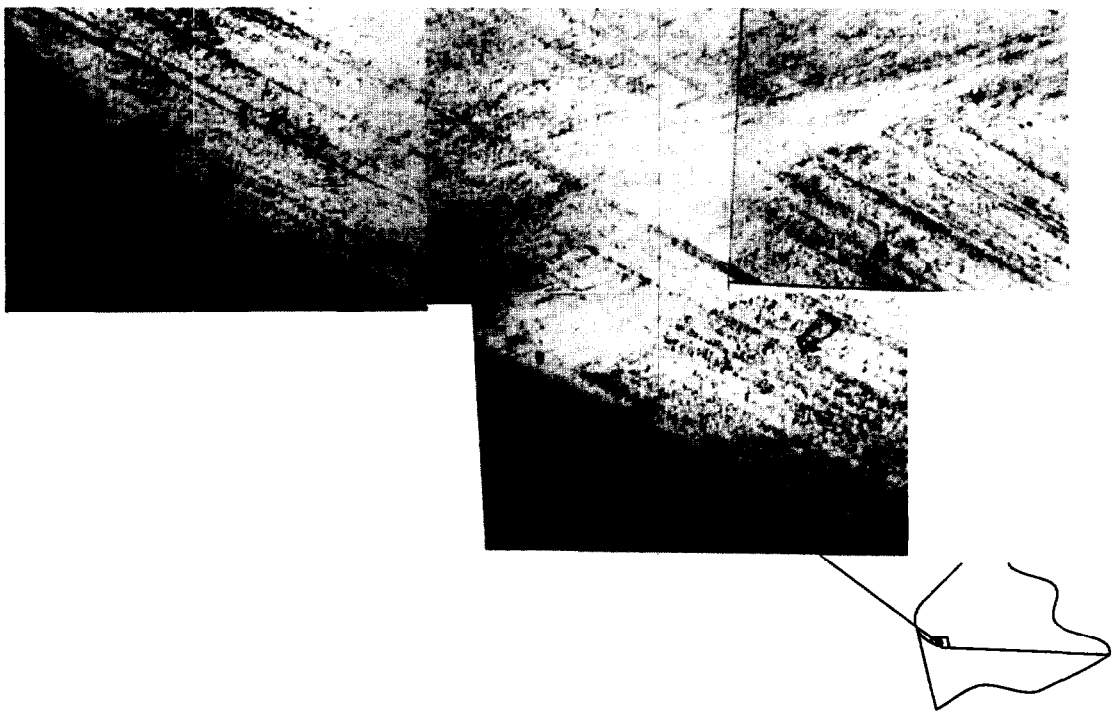

Fig. 9. Photomicrograph of residual copper layer on rake face.

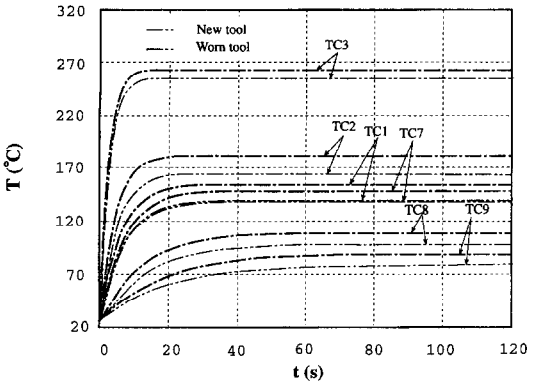

Fig. 10. Wear effects on the temperature profile.

Figure 10 shows a comparison of temperature distributions at various locations in a new and worn tool under the cutting condition of $V = 1.93$ m s^{-1}, $f = 0.11$ mm rev^{-1}, and $w = 0.25$ mm. Temperatures are higher in the worn tool (after in use for 2 h) than in the new one, as expected. One may refer to the thermogram (Fig. 5.9 in [6]) of the worn tool with a nose radius wear of 1 mm and grooves in flank face near the nose radius. The cutting heat transfer into the worn tool is larger due to its contact with larger tool–chips or the tool–finished surface interface formed from the wear zone.

CONCLUSIONS

Experiments have been conducted to measure timewise temperature variations in carbide inserts in cutting cast iron, AISI 1045 steel, copper and 6061 aluminum. A semi-empirical formula has been derived from correlation of cutting data. The time constant and a parameter C determine the temperature–time history of the cutting tool and consequently the tool-wear rate. Measurements by means of thermocouples indicate oscillations in temperatures at the locations near the cutting, more rigorous for the ductile materials and less in the hard-machining materials. It is attributed to the chip formation which raises the local temperature upon its contact with the work material. A tall spike in the temperature response curves, as seen in cutting the ductile materials, results from a chip with minute and irregular corrugations temporarily stuck on the tool surface. That is why cast iron has less of a fluctuation in its temperature response curve and also no tendency to form craters on the tool face end.

Two kinds of wear have been identified from a plot of the steady-state temperature (after transient temperature change ceases) in the four work pieces against the cutting speed: mechanical wear in the lower cutting-speed zone and diffusion wear in the higher cutting-speed zone. The critical value of cutting speeds for the transition from mechanical to diffusion wear is lower in the ductile materials, 2 m s^{-1} for a feed of 0.05 mm rev^{-1} and a depth of cut of 0.25 mm. This critical cutting speed is expected at a higher value in the ferrous materials (not covered in the present study). The rate of decrease in tool life is faster in the mechanical wear zone and slower in the diffusion wear zone.

Infrared thermovision has been employed to visualize and simultaneous, real-time thermal-image processing has quantitatively evaluated timewise change in the global temperature distribution over the surfaces of the cutting tool, workpiece and chip. Results are in good agreement with those obtained by thermocouple measurements. The maximum temperature has been found on the rake face not on the cutting edge of the tool, but a location slightly inward due to the interaction of heat transfer from three heat sources induced by the cutting operation, namely the primary and secondary deformation zones and the tool–workpiece contact surface. The temperature gradient on the rake face is very steep around the maximum temperature point. Microscopic investigation has been performed by means of an optical and electronic microscope in the post-cutting stage. It has been disclosed that (i) the direction of chip flow can be identified through observation of the adhering metal flow on the rake face, and (ii) the surface temperature has reached certain level to produce black cavities, called micropits, which are formed from whole grains or fragments of carbon grains being broken away. Both the number and size of micropits progressively increase as the cutting operation continues, eventually causing groove wear and crater wear depending on the location of surface damage on the cutting tool.

REFERENCES

1. Moriwaki, T., Horiuchi, A. and Okuda, K., Effect of cutting heat on machining accuracy in ultra-precision diamond turning. *CIRP Annals*, 1990, **39**, 81–84.
2. Nakai, T., Nakatani, S., Tomita, K. and Goto, M., Hard turning by PCBN. *Society of Manufacturing Engineers*, 1991, Technical Paper MR91-190.
3. Stovicek, D., Hard part turning. *Tooling and Production*, 1992, **57**(2), 25–26.
4. Subramani, G., Kapoor, S. G. and DeVor, R. E., A model for the prediction of bore cylindricity during machining. *ASME Journal of Engineering for Industry*, 1993, **115**, 15–22.
5. Stephenson, D. A., Barone, M. R. and Dargush, G. F., Thermal expansion of the workpiece in turning. *Materials Issues in Machining—II and The Physics of Machining Processes—II*, ed. D. A. Stephenson and R. Stevenson. *ASME*, New York, 1994, pp. 257–279.
6. Ay, H., Heat transfer and life of cutting tool in turning. Ph. D. dissertation, University of Michigan, Ann Arbor, MI, 1995.
7. Gottwein, K., Die Messung der Schneidentemperatur bein Abdrehen von Flusseisen. *Maschinenbau*, 1925, **4**, 1129–1135.
8. Herbert, E. G., The measurement of cutting temperature. *Proceedings of Institution of Mechanical Engineers*, Vol. 1, 1926, pp. 289–329.
9. Braiden, P. M., Measurement of transient surface temperatures in metal cutting. *Proceedings of Institution of Mechanical Engineers*, Vol. 182, 1967–68 (3G), pp. 68–70.

10. Küsters, K. J., Ph.D dissertation, T. H. Aachen, 1956.
11. Usui, E., Shirakashi, T. and Kitagawa, T., Analytical prediction of three-dimensional cutting process Part 3 cutting temperature and crater wear of carbide tool. *ASME Journal of Engineering for Industry*, 1978, **100,** 236–243.
12. Schwerd, F. Z., Über die Bestimmung des Temperaturfeldes Beim Spanablauf. *Zeitschrift des Vereines Deutscher Ingenieure*, 1937, **77,** 211–216.
13. Hollander, M. B., An infra-red microradiation technique investigation of the temperature distribution in the workpiece during cutting. *A.S.T.E. Report* no. 21, 1959.
14. Chao, B. T., Li, H. L. and Trigger, K. J., An experimental investigation of temperature distribution at the tool flank surface. *ASME Series B*, 1961, **83,** 496–504.
15. Trigger, K., Temperatures in machining and their importances. *International Production Engineering Research Conference, ASME*, New York, 1963, pp. 95–101.
16. Boothroyd, G., Temperature in orthogonal metal cutting. *Proceedings of Institution of Mechanical Engineers*, Vol. 177, No. 29, 1963, pp. 789–810.
17. Bickel, E. and Widmer, W., The temperature on the cutting edge. *Industrial Organization*, 1954, **8.**
18. Lenz, E., What temperatures do we get. *SME/CCPA Conference*, Paper no. MR71-905, 1971.
19. Belcher, P. R. and Wilson, R. W., Templugs. *The Engineer*, 1966, **221,** 305–308.
20. Smart, E. F. and Trent, E. M., Temperature distribution in tools used for cutting iron, titanium and nickel. *International Journal of Production Research*, 1975, **13,** 265–290.
21. Schallbrock, H. and Lang, M. Z., Messung der Schnittemperatur mitlels Temperaturanzeigender Farbanstriche. *Zeitschrift des Vereines Deutscher Ingenieure*, 1943, **87,** 15–32.
22. Pahlitzsch, G. and Helmerdig, H., Das Temperaturfeld am Drehmeibol wärmetechnisch Betrachtee. *Zeitschrift des Vereines Deutscher Ingenieure*, 1943, **87,** 564–576 and 691–704.
23. Ay, H., Yang, W.-J. and Yang, J.A., Dynamics of cutting tool temperatures during cutting process. *Experimental Heat Transfer*, 1994, **7**(3).
24. Ross, Robert B., *Metallic Materials Specification Handbook*. Chapman and Hall, New York, 1992.
25. Boothroyd, G. and Knight, W. A., *Fundamentals of Machining and Machine Tools*, 2nd edn. Marcel Dekker, New York, 1989.